

On reconstruction of small sources from Cauchy data at a fixed frequency

Isaac Harris*

Thu Le[†]Dinh-Liem Nguyen[‡]

Abstract

This short paper is concerned with the numerical reconstruction of small sources from boundary Cauchy data for a single frequency. We study a sampling method to determine the location of small sources in a very fast and robust way. Furthermore, the method can also compute the intensity of point sources provided that the sources are well separated. A simple justification of the method is done using the Green representation formula and an asymptotic expansion of the radiated field for small volume sources. The implementation of the method is non-iterative, computationally cheap, fast, and very simple. Numerical examples are presented to illustrate the performance of the method.

Keywords. inverse source problem, numerical reconstruction, Cauchy data, small sources, single frequency

AMS subject classification. 35R30, 35R09, 65R20

1 Introduction

We study in this paper a numerical method for the inverse source problem of determining small radiating sources from Cauchy data at a fixed frequency. The Cauchy data are boundary measurements of the field generated by the source. Inverse source problems have applications in physics and engineering such as antenna synthesis and medical imaging. These inverse problems have been studied intensively during the past two decades. We refer to [1, 6, 8, 11, 17] and references therein for results on stability analysis of inverse source problems. There has been a large amount of literature on numerical methods for solving these inverse problems. Results on numerical methods for inverse source problems with multi-frequency data can be found in [3, 9, 10, 13–15, 19, 20].

In the case of data associated with a single frequency inverse source problems may have multiple solutions unless some a priori information about the source is given [2, 7]. We refer to [4, 5, 12, 18] for an algebraic method for computing point sources for elliptic partial differential equations such as the Poisson equation and the Helmholtz equation. An iterative approach of Newton type can be found in [2, 16] for recovering point and extended sources. A direct sampling method for computing multipolar point sources for the Helmholtz equation was studied in [21]. The main advantage of the sampling approach is that it is non-iterative, fast, and computationally cheap. In the present work, we also study a sampling method for recovering point sources and small volume sources for the Helmholtz equation. Compared with the imaging functional introduced in [21] the imaging functional in this paper involves only a single integral instead of a double integral. Thus the sampling method in the present work may be faster and computationally cheaper (e.g. for large search domains in three dimensions). In addition, our implementation does not require a multi-level sampling process as in [21] and seems to provide

*Department of Mathematics, Purdue University, West Lafayette, IN 47907, USA; (harri814@purdue.edu)

[†]Department of Mathematics, Kansas State University, Manhattan, KS 66506, USA; (thule@ksu.edu)

[‡]Department of Mathematics, Kansas State University, Manhattan, KS 66506, USA; (dlnghuyen@ksu.edu).

equivalently good reconstruction results. The justification of our sampling method for both two and three dimensions is done simultaneously in a pretty simple way. It relies on the Green representation formula and an asymptotic expansion of the radiated field for small volume sources.

The paper is organized as follows. Section 2 is dedicated to the reconstruction of the location and intensity of point sources. The method is extended to locate sources with small volumes in Section 3. A numerical study of the performance of the method is presented in Section 4.

2 Reconstruction of point sources

We consider $N \in \mathbb{N}$ point sources located at x_j for $j = 1, 2, \dots, N$ such that $\text{dist}(x_i, x_j) \geq c_0 > 0$. These sources are represented by the Delta distributions δ_{x_j} and have nonzero intensities $\alpha_j \in \mathbb{C}$. Let $k > 0$ be the wavenumber. Assume that the sources generate the radiating scattered field u that satisfies the following model problem

$$\Delta u + k^2 u = - \sum_{j=1}^N \alpha_j \delta_{x_j}, \quad \text{in } \mathbb{R}^d, \quad (1)$$

$$\lim_{r \rightarrow \infty} r^{\frac{d-1}{2}} \left(\frac{\partial u}{\partial r} - iku \right) = 0, \quad r = |x|, \quad (2)$$

where $d = 2$ or 3 is the dimension and the Sommerfeld radiation condition (2) holds uniformly for all directions $\hat{x} \in \{\hat{x} \in \mathbb{R}^d : |\hat{x}| = 1\}$. The radiating scattered field u is given by

$$u(x) = \sum_{j=1}^N \alpha_j \Phi(x, x_j), \quad (3)$$

where $\Phi(x, y)$ is the Green function of problem (1)–(2)

$$\Phi(x, y) = \begin{cases} \frac{i}{4} H_0^{(1)}(k|x-y|), & \text{in } \mathbb{R}^2, \\ \frac{e^{ik|x-y|}}{4\pi|x-y|}, & \text{in } \mathbb{R}^3, \end{cases} \quad (4)$$

and $H_0^{(1)}$ is the first kind Hankel function of order zero. Let Ω be a regular bounded domain with boundary $\partial\Omega$ in \mathbb{R}^d . Assume that $x_j \in \Omega$ for $j = 1, \dots, N$ and denote by $\nu(x)$ the outward normal unit vector to $\partial\Omega$ at x .

Inverse problem: Given the Cauchy data u and $\partial u / \partial \nu$ on $\partial\Omega$ for a fixed wave number k , determine locations x_j and intensities α_j for $j = 1, 2, \dots, N$.

We note that with a single wave number k the Cauchy data is important to justify the uniqueness of solution to this inverse problem, see [2, 7]. The following simple lemma is important for the resolution analysis of the imaging functional we study for the inverse source problem.

Lemma 1. *The following identity holds for the radiating scattered field u in (3)*

$$\int_{\partial\Omega} \left(\frac{\partial \text{Im } \Phi(x, z)}{\partial \nu(x)} u(x) - \text{Im } \Phi(x, z) \frac{\partial u(x)}{\partial \nu(x)} \right) ds(x) = \sum_{j=1}^N \alpha_j \text{Im } \Phi(x_j, z). \quad (5)$$

Proof. Substituting the formula for u in (3) in the left hand side of (14) implies

$$\begin{aligned} & \int_{\partial\Omega} \left(\frac{\partial \text{Im } \Phi(x, z)}{\partial \nu(x)} \sum_{j=1}^N \alpha_j \Phi(x, x_j) - \text{Im } \Phi(x, z) \sum_{j=1}^N \alpha_j \frac{\partial \Phi(x, x_j)}{\partial \nu(x)} \right) ds(x) \\ &= \sum_{j=1}^N \alpha_j \int_{\partial\Omega} \left(\frac{\partial \text{Im } \Phi(x, z)}{\partial \nu(x)} \Phi(x_j, x) - \text{Im } \Phi(x, z) \frac{\partial \Phi(x_j, x)}{\partial \nu(x)} \right) ds(x). \end{aligned} \quad (6)$$

Due to the fact that $\Delta \text{Im } \Phi(z, y) + k^2 \text{Im } \Phi(z, y) = 0$ for all $z, y \in \mathbb{R}^d$ the proof follows from the Green representation formula i.e.

$$\int_{\partial\Omega} \left(\frac{\partial \text{Im } \Phi(x, z)}{\partial \nu(x)} \Phi(y, x) - \text{Im } \Phi(x, z) \frac{\partial \Phi(y, x)}{\partial \nu(x)} \right) ds(x) = \text{Im } \Phi(y, z)$$

which proves the claim. \square

Now, we define the imaging functional

$$I(z) := \int_{\partial\Omega} \left(\frac{\partial \text{Im } \Phi(x, z)}{\partial \nu(x)} u(x) - \text{Im } \Phi(x, z) \frac{\partial u(x)}{\partial \nu(x)} \right) ds(x), \quad z \in \mathbb{R}^d. \quad (7)$$

Therefore, from the lemma above we have that

$$I(z) = \sum_{j=1}^N \alpha_j \text{Im } \Phi(x_j, z),$$

where

$$\text{Im } \Phi(x, z) = \begin{cases} \frac{1}{4} J_0(k|x-z|) & \text{in } \mathbb{R}^2, \\ \frac{k}{4\pi} j_0(k|x-z|) & \text{in } \mathbb{R}^3, \end{cases} \quad (8)$$

and J_0 and j_0 are respectively a Bessel function and a spherical Bessel function of the first kind.

We know from (8) that $\text{Im } \Phi(z, x_j)$ peaks at $z \approx x_j$ and decays as z is away from x_j . Thus we can determine N as the number of significant peaks of $|I(z)|^p$ where $p > 0$ is chosen to sharpen the significant peaks of the imaging functional (e.g. $p = 4$ works well for the numerical examples in the last section). Then x_j can be determined as the locations where $|I(z)|^p$ has significant peaks. It is obvious that the resolution for imaging the sources is within the diffraction limit. Furthermore, from the fact

$$J_0(t) = \mathcal{O}(t^{-1/2}) \quad \text{and} \quad j_0(t) = \mathcal{O}(t^{-1})$$

as $t \rightarrow \infty$, we have

$$|I(z)|^p = \mathcal{O}\left(\text{dist}(z, X)^{\frac{(1-d)p}{2}}\right) \quad \text{as} \quad \text{dist}(z, X) \rightarrow \infty$$

where the set $X = \{x_j : 1, \dots, N\}$. Moreover, once x_j is obtained the intensity α_j can be estimated as

$$\alpha_j \approx \frac{I(x_j)}{\text{Im } \Phi(x_j, x_j)} \quad \text{since the } x_j \text{'s are well separated.} \quad (9)$$

It is easy to verify that the imaging functional is stable with respect to noise in the Cauchy data see for instance [21]. We leave the proof to the readers.

3 Reconstruction of small volume sources

We let D with Lipschitz boundary ∂D have small volume in \mathbb{R}^d such that $|D| = \mathcal{O}(\epsilon^d)$. To this end, we assume that the scatterer D is given by a collection of small volume subregions i.e.

$$D = \bigcup_{j=1}^N D_j \quad \text{with} \quad D_j = (x_j + \epsilon B_j) \quad \text{such that} \quad \text{dist}(x_i, x_j) \geq c_0 > 0 \quad (10)$$

for $i \neq j$ where the parameter $0 < \epsilon \ll 1$ and B_j is a radially symmetric domain with Lipschitz boundary centered at the origin such that $|B_j|$ is independent of ϵ . We also assume that the D_j are pairwise disjoint

such that $D_j \cap D_i$ is empty for $i \neq j$. Let $f \in L^2(D)$ where $\mathbb{1}_D$ denotes the indicator function on the set D . We assume that the radiating scattered field $u \in H_{loc}^1(\mathbb{R}^d)$ generated by these small sources satisfies

$$\Delta u + k^2 u = -f \mathbb{1}_D \quad \text{in } \mathbb{R}^d \quad (11)$$

along with the Sommerfeld radiation condition as in (2). It is well-known that the solution is given by

$$u(x) = \int_D f(y) \Phi(x, y) \, dy \quad (12)$$

where $\Phi(x, y)$ is the Green function as in (4).

We consider inverse problem of determining x_j , $j = 1, \dots, N$, from u and $\partial u / \partial \nu$ on $\partial \Omega$. We have that for any $x \in \mathbb{R}^d \setminus \overline{D}$ we can use a first order Taylor expansion of the Green function to approximate the radiated field u . Therefore, we notice that $y \in D_j$ if and only if $y = x_j + \epsilon \omega$ for some $\omega \in B_j$ which gives that

$$\begin{aligned} u(x) &= \int_D f(y) \Phi(x, y) \, dy = \sum_{j=1}^N \int_{D_j} f(y) \Phi(x, x_j + \epsilon \omega) \, dy \\ &= \sum_{j=1}^N \left(\Phi(x, x_j) + \mathcal{O}(\epsilon) \right) \int_{D_j} f(y) \, dy. \end{aligned}$$

Then, letting \overline{f}_{D_j} be the average value of f on D_j and using the fact that $|D_j| = \epsilon^d |B_j|$ we have that

$$u(x) = \epsilon^d \sum_{j=1}^N \overline{f}_{D_j} |B_j| \Phi(x, x_j) + \mathcal{O}(\epsilon^{d+1}). \quad (13)$$

This gives that up to leading order u acts like a radiating scattered field generated by point sources located at x_j with intensity $\alpha_j = \epsilon^d |B_j| \overline{f}_{D_j}$. Notice, that by the Cauchy-Schwartz inequality we have that is bounded with respect to ϵ . As in (14), we use (13) and the Green formula for $\text{Im } \Phi(x, z)$ to derive the following identity.

Lemma 2. *The following identity holds for the radiating scattered field u in (3)*

$$\int_{\partial \Omega} \left(\frac{\partial \text{Im } \Phi(x, z)}{\partial \nu(x)} u(x) - \text{Im } \Phi(x, z) \frac{\partial u(x)}{\partial \nu(x)} \right) \, ds(x) = \epsilon^d \sum_{j=1}^N \overline{f}_{D_j} |B_j| \text{Im } \Phi(x_j, z) + \mathcal{O}(\epsilon^{d+1}). \quad (14)$$

As in the case of point sources this lemma allows us to use the imaging functional $I(z)$ in (7) to determine x_j . In fact, the centers x_j of the small sources can be determined as the locations where $|I(z)|^p$ has significant peaks. And also, up to the leading order, if $\overline{f}_{D_j} \neq 0$ we have that for all $z \in \mathbb{R}^d \setminus \overline{D}$, $|I(z)|^p = \mathcal{O}\left(\text{dist}(z, X)^{\frac{(1-d)p}{2}}\right)$ as $\text{dist}(z, X) \rightarrow \infty$ where the set $X = \{x_j : 1, \dots, N\}$.

4 Numerical examples

We present some numerical examples in two dimensions to demonstrate the performance of the method. In all of the numerical examples the wave number is chosen as $k = 20$ and the Cauchy data is given at 256 points which are uniformly distributed on the circle centered at the origin with a radius of 50 (which is about 159 wavelengths). The data is computed using equations (3) and (12), respectively with 10% random noise added to the data. The noise vectors $\mathcal{N}_{1,2}$ consist of numbers $a + ib$ where $a, b \in (-1, 1)$

are randomly generated with a uniform distribution. For simplicity we consider the same noise level for both u and $\partial u/\partial \nu$. The noise vectors are added to u and $\partial u/\partial \nu$ as follows

$$u + 10\% \frac{\mathcal{N}_1}{\|\mathcal{N}_1\|_F} \|u\|_F, \quad \frac{\partial u}{\partial \nu} + 10\% \frac{\mathcal{N}_2}{\|\mathcal{N}_2\|_F} \left\| \frac{\partial u}{\partial \nu} \right\|_F,$$

where $\|\cdot\|_F$ is the Frobenius matrix norm. The imaging functional $I(z)$ is computed at 256×256 uniformly distributed sampling points on the search domain $[-2, 2]^2$. That means the distance between two consecutive sampling points is about 0.05 wavelength. This distance is small enough since the sources are supposed to be well separated.

The reconstruction results for the location and intensity of different numbers of point sources can be seen in Tables 1 and 2 as well as Figure 1. The number of significant peaks of $|I(z)|^4$ (i.e. $p = 4$) can be seen clearly in Figure 1. Then we determine x_j as the location of these peaks. Tables 1 and 2 show that the locations x_j of the sources δ_{x_j} ($j = 1, \dots, N$) are computed with good accuracy and the intensities α_j are recovered with reasonable errors (the relative error ranges from 1% to 10%). In particular, the method can reasonably compute the location and intensity of two point sources located within a wavelength. It is noticed that the error gets worse as the number of sources to compute increases. We display in Table 3 and Figure 2 the reconstruction results of sources that are small disks. The centers x_j of these circular sources are again computed with very good accuracy.

Table 1: Reconstruction result for the location of N point sources

N	True location x_j	Computed location x_j
2 (close)	(0.15, 0), (-0.15, 0)	(0.125, 0.000), (-0.125, 0.000)
2 (distant)	(-1, 0.8), (0.7, -1)	(-1.000, 0.796), (0.703, -1.000)
3	(1, -1), (1.3, 1), (-1.2, -0.25)	(1.000, -0.984), (-1.312, 0.984), (-1.203, -0.250)
4	(1, -1), (1, 0.75), (-1.2, -1), (-1.2, 0.75)	(1.015, -1.000), (1.015, 0.750), (-1.203, -1.000), (-1.203, 0.750)

Table 2: Reconstruction result for the intensity of N point sources with location in Table 1

N	True intensity α_j	Computed intensity α_j
2 (close)	$1 - 2i, 1 + 2i$	$0.942 - 1.881i, 0.950 + 1.899i$
2 (distant)	$1 - 2i, 1 + 2i$	$1.007 - 2.045i, 1.024 + 2.004i$
3	$4 + 0i, 3.5 - i, 3.5 + i$	$3.912 + 0.023i, 3.431 - 0.918i, 3.570 + 0.968i$
4	$2.5 + 2i, 2.5 - 2i, 3.5 - i, 3 + i$	$2.725 + 2.237i, 2.759 - 2.158i, 3.532 - 1.035i, 2.982 + 1.077i$

Table 3: Reconstruction result for the center x_j of N small disks

N	True x_j	Computed x_j
3	(1, 0.75), (-1, -1), (1.25, -1.5)	(0.984, 0.734), (-0.984, -1.000), (1.234, -1.500)
4	(1, 1), (-1, -1.25), (1, -1), (-1, 0.75)	(0.984, 0.984), (-0.984, -1.234), (0.984, -0.984), (-0.984, 0.734)
5	(1.25, 1.2), (-1, 0), (1, -1), (-0.6, 1), (0.25, 0)	(1.265, 1.203), (-1.000, 0.015), (1.000, -1.015), (-0.609, 0.984), (0.250, 0.000)

Acknowledgments: The work of I. Harris was partially supported by the NSF Grant DMS-2107891. The work of T. Le and D.-L. Nguyen was partially supported by NSF Grant DMS-2208293.

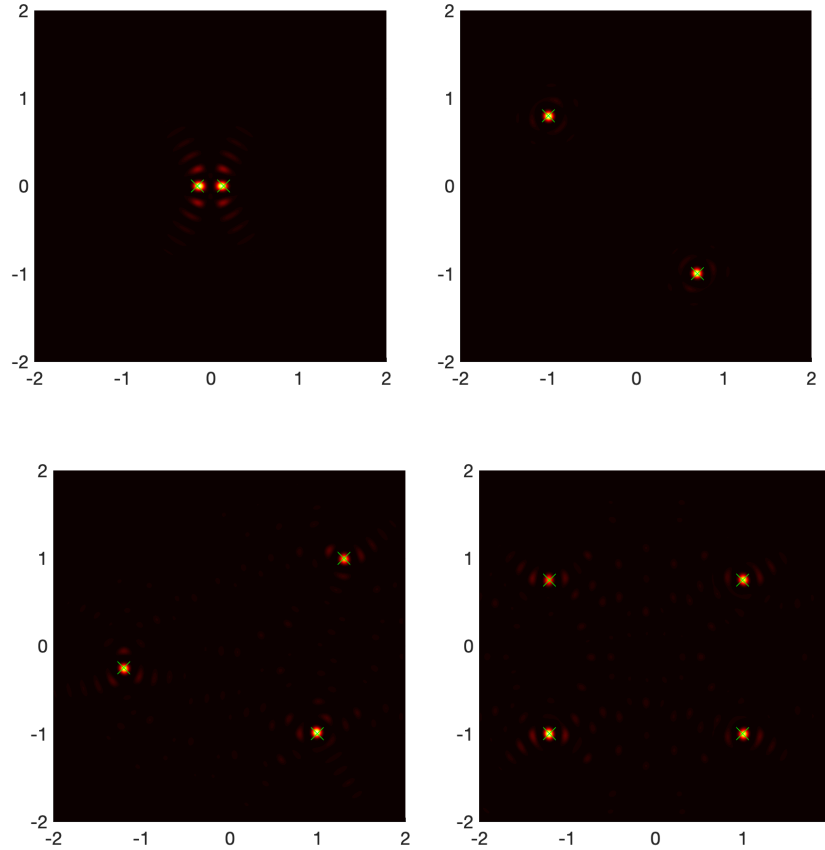


Figure 1: Pictures of $|I(z)|^4$ for point sources. The true location of the sources are displayed by the green crosses.

References

- [1] S. Acosta, S. Chow, J. Taylor, and V. Villamizar. On the multi-frequency inverse source problem in heterogeneous media. *Inverse Problems*, 28:075013, 2012.
- [2] C. Alves, R. Kress, and P. Serranho. Iterative and range test methods for an inverse source problem for acoustic waves. *Inverse Problems*, 25:055005 (17pp), 2009.
- [3] A. Alzaalig, G. Hu, X. Liu, and J. Sun. Fast acoustic source imaging using multi-frequency sparse data. *Inverse Problems*, 36:025009, 2020.
- [4] A. El Badia. Inverse source problem in an anisotropic medium by boundary measurements. *Inverse Problems*, 21:1487–506, 2005.
- [5] A. El Badia and T. Ha-Duong. An inverse source problem in potential analysis. *Inverse Problems*, 16:651–63, 2000.
- [6] A. El Badia and A. El Hajj. Stability estimates for an inverse source problem of helmholtz equation from single cauchy data at a fixed frequency. *Inverse Problems*, 29:125008, 2013.
- [7] A. El Badia and T. Nara. An inverse source problem for Helmholtz’s equation from the Cauchy data with a single wave number. *Inverse Problems*, 27:105001, 2011.

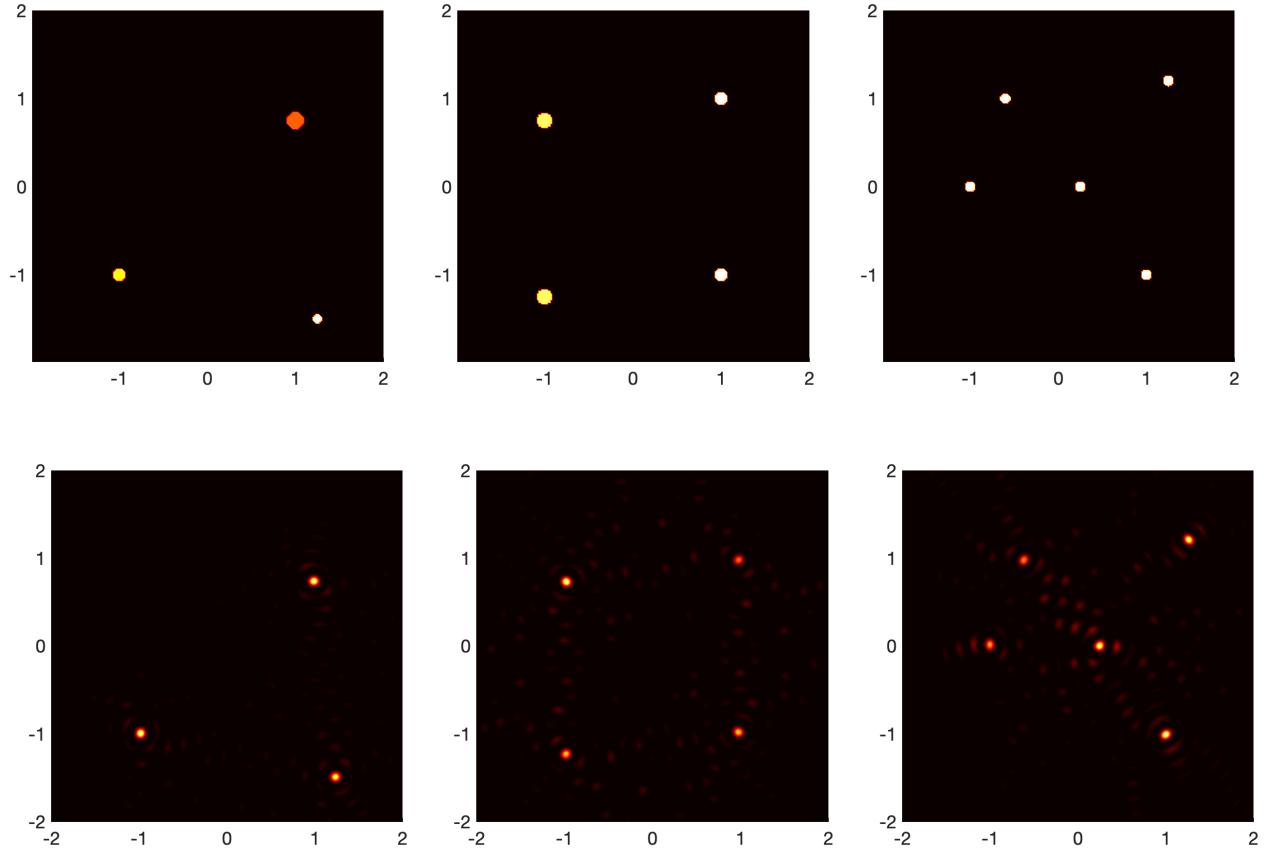


Figure 2: The first row is the true profile of small volume sources (the color of the disks is associated with the value of f on each disk that we are not able to recover using $I(z)$). The second row contains pictures of $|I(z)|^4$.

- [8] G. Bao, P. Li, and Y. Zhao. Stability for the inverse source problems in elastic and electromagnetic waves. *J. Math. Pures Appl.*, 134:122–178, 2020.
- [9] G. Bao, J. Lin, and F. Triki. Numerical solution of the inverse source problem for the helmholtz equation with multiple frequency data. *Contemp. Math., AMS*, 548:45–60, 2011.
- [10] G. Bao, S. Lu, W. Rundell, and B. Xu. A recursive algorithm for multifrequency acoustic inverse source problems. *SIAM J. Numer. Anal.*, 53:1608–1628, 2015.
- [11] J. Cheng, V. Isakov, and S. Lu. Increasing stability in the inverse source problem with many frequencies. *J. Differential Equations*, 260:4786–4804, 2016.
- [12] Y.-S. Chung and S.-Y. Chung. Identification of the combination of monopolar and dipolar sources for elliptic equations. *Inverse Problems*, 25:085006, 2009.
- [13] M. Eller and N. Valdivia. Acoustic source identification using multiple frequency information. *Inverse Problems*, 25:115005, 2009.
- [14] R. Griesmaier and C. Schmiedecke. A factorization method for multifrequency inverse source problems with sparse far field measurements. *SIAM J. Imaging Sciences.*, 10:2119–2139, 2017.
- [15] X. Ji. Reconstruction of multipolar point sources with multi-frequency sparse far field data. *Inverse Problems*, 37:065015 (18pp), 2021.

- [16] R. Kress and W. Rundell. Reconstruction of extended sources for the helmholtz equation. *Inverse Problems*, 29:035005, 2013.
- [17] P. Li, J. Zhai, and Y. Zhao. Lipschitz stability for an inverse source scattering problem at a fixed frequency. *Inverse Problems*, 37:025003, 2021.
- [18] T. Nara. An algebraic method for identification of dipoles and quadrupoles. *Inverse Problems*, 24:025010, 2008.
- [19] L. H. Nguyen, Q. Li, and M. Klibanov. A convergent numerical method for a multi-frequency inverse source problem in inhomogeneous media. *Inverse Probl. Imaging*, 13:1067–1094, 2019.
- [20] D. Zhang and Y. Guo. Fourier method for solving the multi-frequency inverse source problem for the Helmholtz equation. *Inverse Problems*, 31:035007, 2015.
- [21] D. Zhang, Y. Guo, J. Li, and H. Liu. Locating multiple multipolar acoustic sources using the direct sampling method. *Commun. Comput. Phys.*, 25:1328–1356, 2019.